Article:

Olanrewaju, FO, Li, H, Aslam, Z et al. (2 more authors) (2022) Analysis of the effect of syngas substitution of diesel on the Heat Release Rate and combustion behaviour of Diesel-Syngas dual fuel engine. Fuel, 312. 122842. ISSN 0016-2361

https://doi.org/10.1016/j.fuel.2021.122842

Analysis of the Effect of Syngas Substitution of Diesel on the Heat Release Rate and Combustion Behaviour of Diesel-Syngas Dual Fuel Engine

Francis Omotola Olanrewaju[a,b*], Hu Li[a], Zahida Aslam[a], James Hammerton[a] and Jon C. Lovett[c]

[a]School of Chemical and Process Engineering, Faculty of Engineering and Physical Sciences, University of Leeds, LS2 9JT, United Kingdom
[b]Department of Engineering Infrastructure, National Agency for Science and Engineering Infrastructure (NASENI), Abuja, Nigeria
[c]School of Geography, University of Leeds, LS2 9JT, United Kingdom

Abstract

The Heat Release Rate (HRR) model of ICEs is known to be most sensitive to the ratio of specific heats, γ, which is known to be depended on temperature and the excess air ratio, λ. The HRR of ICEs cannot be measured directly. As such, accurate HRR models, as well as accurate expressions of γ and λ are required to model the HRR behaviour of ICEs mathematically. In this work, an improved HRR model based on $\gamma(T,\lambda)$ was used to investigate the effect of syngas substitution of diesel at constant energy on the Heat Release Rate (HRR) behaviour and the combustion phasing in a 5.7 kW engine out and 4.3 kW generator output, single cylinder, dual fuel, Reactivity Controlled Compression Ignition (RCCI) mode CI engine. An improved global excess air ratio, λ_g was used in the HRR analysis of the dual fuel engine. The engine was run on 10, 25, and 45% syngas substitution (by energy) and at 1, 2, 3, and 4 kW loads (generator output) for each syngas substitution. The improved dual fuel engine HRR model was validated by comparing the measured fuel consumption by energy (input energy) per (thermodynamic) cycle to the predicted fuel consumption by energy per cycle for the tested conditions. The values of the fuel consumption predicted by the Leeds HRR model were also compared to the predictions of the HRR models that were based on

* Corresponding author. Tel.: +447503114068; +2347030285759
E-mail addresses: pmofo@leeds.ac.uk; sonictreasure@gmail.com (F.O. Olanrewaju), h.li3@leeds.ac.uk (H. Li), pmzba@leeds.ac.uk (Z. Aslam), j.m.hammerton@leeds.ac.uk (J. Hammerton), J.Lovett@leeds.ac.uk (J. C. Lovett)

$\gamma(T)$. The overall average error in the predictions of the fuel input energy by the Leeds HRR model was 2.41% with a standard deviation of 1.65. The overall average errors in the other models ranged from 6.26 to 8.29%. The SoC, MFB50, PP, and PHRR occurred later for the diesel-syngas dual fuels compared to baseline diesel due to increased ignition delay as the fraction of syngas was increased. The current work showed that the use of diesel-syngas dual fuel in diesel engines in Nigeria (a developing country) can potentially reduce CO_2 emissions by up to ~0.26 million tonnes.

Key words: Dual-fuel engine, combustion, syngas, RCCI, global lambda, modelling

Nomenclature

Symbols:

A_s	Surface area
b	Coefficients of ratio of specific heats function for burned mixtures
c_m	Mean piston speed
c_p	Specific heat capacity at constant pressure
c_v	Specific heat capacity at constant volume
h	Heat transfer coefficient
h_{bb}	Enthalpy of blow-by gases
K_1	Constant
m	Amount of gas in cylinder
$\dot{m}$	Mass flow rate
m_{bb}	Mass of blow–by gases
m_f	Mass of injected fuel
p	Pressure
$p',\ p''$	Differentials of pressure
Q	Heat released from injected fuel
Q_b	Heat loss through blow–by gases

Q_w	Heat loss through cylinder walls
q_e	Heat of evaporation of fuel
R	Universal gas constant
R'	Ratio of length of connecting rod to crank radius
r	Compression ratio
T	Temperature
V	Volume
W	Pressure–volume work

Greek symbols:

γ	Specific heats ratio
δ	Blow-by gap
k_1, k_2	Constants
λ	Excess air ratio
ϕ	Equivalence ratio
π	Constant
ρ	Density
θ	Crank Angle Degree

Subscripts:

bb	Blow–by
d	Displaced
e	Evaporation
eff	Effective
g	Global
m	Mean
mod	Modified
ref	Reference

s	Surface
$stoich$	Stoichiometric
w	Wall

Abbreviations:

AFR	Air Fuel Ratio
aTDC	After Top Dead Centre
bTDC	Before Top Dead Centre
CAD	Crank Angle Degree
CHR	Cumulative Heat Release
CI	Compression Ignition
CN	Cetane Number
Cv	Calorific value
DI	Direct Injection
DoC	Duration of Combustion
EGR	Exhaust Gas Recirculation
EoC	End of Combustion
EVC	Exhaust Valve Closing
GTL	Gas-to-Liquid
HRR	Heat Release Rate
HVO	Hydrotreated Vegetable Oil
ICE	Internal Combustion Engine
ID	Ignition Delay
IMEP	Indicated Mean Effective Pressure
IVC	Intake Valve Closing
LTC	Low Temperature Combustion
MFB	Mass Fraction Burned
MFIS	Multiple Fuel Injection Strategy
PHRR	Peak Heat Release Rate

PP	Peak Pressure
PT	Peak Temperature
RCCI	Reactivity Controlled Compression Ignition
rpm	Revolutions per minute
SG	Diesel-syngas dual fuel
SoC	Start of Combustion
ULSD	Ultra Low Sulphur Diesel

1. Introduction

The utilization of syngas in diesel generators will widen the fuel choices and availability in those developing countries with abundant biomass to produce syngas [1]. Fossil fuels require large-scale refining and transport infrastructure, and are also subject to geopolitical events that can affect social stability, price and availability [2,3]. Diesel supply is limited in many rural and remote areas creating a constraint to sustainable development. Diesel-syngas dual fuel is beneficial and desirable in developing countries because it provides alternative fuel sources and enhances the use of renewable fuels for electricity generation. The use of diesel-syngas dual fuel for electricity generation can be achieved through Reactivity Controlled Compression Ignition (RCCI) technology.

RCCI technology is a combustion technology that involves the utilization of at least two fuels of different reactivities to optimize the phasing of the combustion in Compression Ignition (CI) engines. The use of two fuels of different reactivities or Cetane Number (CN) in CI engines has the potential to reduce the Peak Pressure Rise Rate (PPRR), the Peak Heat Release Rate (PHRR), the Peak Pressure (PP), and the Peak Temperature (PT). Therefore, RCCI is a Low Temperature Combustion (LTC) technology that can potentially reduce engine-out NOx emissions. The determination and optimization of the combustion phasing of diesel-syngas dual-fuel RCCI engines require accurate Heat Release Rate (HRR) models. The HRR models of ICEs are based on the First Law of thermodynamics [4]. The accuracy of the HRR models of Internal Combustion Engines (ICEs) is strongly depended on the specific heats ratio (γ). The specific heats ratio, γ on the other hand has been shown to be strongly depended on the temperature (T) of the gases in the cylinder as well as the excess air ratio (λ) [5]. Therefore, accurate models (expressions) of λ are also required in HRR analysis. The Leeds HRR model has been validated for liquid fuels: pure diesel as well as alternative diesels: Gas-to-Liquid (GTL) diesel and Hydrotreated Vegetable Oil (HVO) diesel [5,6]. The improved accuracy of the Leeds HRR model is mainly due to the expression of γ as a function of T and λ. The aim of the current work was to validate and apply the Leeds HRR model to diesel-syngas dual-fuel combustion in an RCCI engine. The current work was carried out on a 5.7 kW, single cylinder, RCCI mode engine with a modern combustion chamber design (re-entrant bowl piston). Notwithstanding, the model results here presented are generally applicable to RCCI mode diesel-syngas dual-fuel engines.

1.1 Previous works on diesel-syngas dual fuel HRR analysis

The effect of simulated syngas substitution of diesel on the combustion characteristics and engine performance was investigated by Garnier et al. [7] using a Litter-Petter diesel engine. The authors validated their HRR model (derived from Wiebe's Law) by comparing it graphically to the model that was derived from the measured pressure-crank angle degree (P-CAD) data. According to the authors, the PHRR decreased in the first stage of the combustion when the pilot fuel (diesel) was <45-50%. The authors reported that the Ignition Delay (ID) decreased as the syngas substitution increased. Le Anh and Hoang [8] studied the effect of diesel-syngas dual fuel on a 3-cylinder, 8.75 kW diesel engine. The authors utilized real syngas in their work and reported that the HRR of the engine increased as the flow of syngas was increased. The authors attributed this to the high flame speed of the hydrogen and the carbon monoxide components of the tested syngas. According to the authors, the engine-out CO increased as the ratio of syngas increased in the dual fuel. The maximum substitution of diesel that was reported was 60% at the investigated engine condition (1,500 rpm and an Indicated Mean Effective Pressure (IMEP) of 6.54 bar).

Le Anh and Hoang [8] utilized the flow rates of diesel, syngas, and air to evaluate the global excess air ratio, as shown in Equation 1.

$$\lambda = \frac{\dot{m}_{air}}{[(\dot{m}_{diesel} \times AFR_{stoich\_diesel}) + (\dot{m}_{syngas} \times AFR_{stoich\_syngas})]} \quad 1$$

$\dot{m}_{air}$, $\dot{m}_{diesel}$, and $\dot{m}_{syngas}$ are the mass flow rates of air, diesel, and syngas respectively, AFR_{stoich} is the stoichiometric air-fuel ratio (AFR). The use of the flow rates in Equation 1 can lead to errors in the estimated values of the global λ because the combustion of fuel in ICEs is a periodic phenomenon.

Guo et al. [9] investigated the effect of syngas fraction and composition on the energy efficiency, cylinder pressure, exhaust temperature, and combustion stability in a 2.44 L, 74.6 kW, single cylinder, diesel engine. Two real syngases and one simulated syngas were used by the authors. The authors reported that the ID and PP increased as the syngas fraction in the dual fuel was increased (contrary to what was reported by Garnier et al. [7]). This underscores the need to further investigate the effect of syngas substitution of diesel on the ID of diesel-syngas dual fuel engines.

Mahgoub et al. [10] investigated the effect of CO_2 removal from a simulated syngas on the performance of syngas dual-fuel engine at 1,850 rpm. A simulated, typical syngas and a simulated high hydrogen syngas were used in the investigation. Biodiesel blend (B50) was used as the direct-injection (pilot) fuel. The authors reported a maximum pilot fuel substitution of 47% with simulated syngas. The authors did not investigate the effect of the dual fuel on the ID of the engine.

Kousheshi et al. [11] investigated the effect of various types of syngas mixtures on the combustion process and the emission characteristics in diesel-syngas RCCI engine using a 2.44 L, single cylinder diesel engine. The HRR of the dual-fuel engine was modelled using a commercial software (CONVERGE). The authors reported that, as the ratio of hydrogen in the syngas increased, the ID decreased, the crank angle at which 50% of the injected fuel was burned (MFB50) was advanced, while the HRR became steeper.

Rith et al. [12] studied the effect of increasing the flow rate of real syngas on the PHRR. The authors utilized a 5.7 kW, single cylinder, naturally aspirated diesel engine in their investigation. The engine was run at 3,000 rpm and 35, 53, and 70% loads. The authors reported that the PHRR decreased and occurred later as the flow rate of the syngas was increased.

The foregoing discussion shows that contradicting results have been reported in literature in terms of the effect of syngas substitution of diesel on the ID of CI engines. Therefore, there is a need to further investigate the effect of syngas substitution of diesel on the phasing of the combustion as well as the ID of CI engines. In the current work, the modified γ function of Ceviz and Kaymaz [13], $\gamma_{mod}(T,\lambda)$ (Equation 2) and the Leeds HRR model developed by Olanrewaju et al. [5] were validated for a 5.7 kW diesel-syngas dual-fuel engine.

$$\gamma_{mod} = b_1 + b_2T + b_3/\lambda + b_4T^2 + b_5/\lambda^2 + b_6T/\lambda + b_7T^3 + b_8/\lambda^3 + + b_9T/\lambda^2 + b_{10}T^2/\lambda \quad 2$$

T in Equation 2 represents the temperature of the gases in the combustion chamber. The values of the constants b_1 to b_{10} in Equation 2 are given in the Appendix as reported by Ceviz and Kaymaz [13].

2. Methodology

2.1 Diesel-syngas dual-fuel engine HRR model development

The Leeds HRR model shown in Equation 3 [5] was adopted in the current work to model the HRR of the diesel-syngas dual-fuel engine.

$$\frac{dQ}{d\theta} = \frac{\gamma}{\gamma-1}p\frac{dV}{d\theta} + \frac{1}{\gamma-1}V\frac{dp}{d\theta} + \frac{dQ_W}{d\theta} + h_{bb}\frac{dm_{bb}}{d\theta} + q_e\frac{dm_f}{d\theta} \quad 3$$

The terms in Equation 3 were explained in the previous works [5,6]. The last term in Equation 3 (heat loss due to the evaporation of the injected fuel mass) was determined in the current work after the HRR and CHR profiles were generated from the basic input data (P-CAD data). The heat absorbed from the combustion chamber to vaporize the injected fuel was estimated by multiplying the product of the total input energy and the fraction of diesel by the ratio of the heat of evaporation and Cv of diesel.

The instantaneous volume of the cylinder, V was calculated from Equation 4 [14].

$$V = (V_d/(r-1)) + (V_d/2)\left[R' + 1 - \cos\theta - \sqrt{R^2 - \sin^2\theta}\right] \qquad 4$$

V_d is the displaced volume, r is the compression ratio, and R' is the ratio of the length of the connecting rod to the crank radius.

The global excess air ratio (λ_g) that was used in Equation 2 was improved by using the trapped masses of air, syngas, and diesel rather than the flow rates as shown in Equation 5.

$$\lambda_g = \frac{m_{air}}{\left[(m_{diesel} \times AFR_{stoich\_diesel}) + (m_{syngas} \times AFR_{stoich\_syngas})\right]} \qquad 5$$

m_{air}, m_{diesel}, and m_{syngas} in Equation 5 represent the trapped masses of air, diesel, and syngas respectively. The volumetric efficiency of the engine for air intake during the intake stroke was determined by experiment as 85%. The ratio of specific heats, γ was estimated by substituting the modified expression for λ_g (Equation 5) into Equation 2.

The Leeds HRR model was validated for the dual-fuel RCCI engine by comparing the predicted fuel input energy per thermodynamic cycle to the input energy per cycle estimated from the injected fuel masses. The predictions of the Leeds HRR model were also compared to those obtained by using the γ functions of Gatowsky et al. [15], Brunt and Emtage [16], Egnell [17], and Blair [18] in the HRR model.

2.2 Model assumptions

The following assumptions were made to apply the improved Leeds HRR model to diesel-syngas dual-fuel RCCI engine:

1. Single zone combustion (combustion parameters were uniform in the cylinder).

2. A zero-dimensional (transient) HRR model.
3. Ideal gas behaviour.
4. The concentration of oxygen in the residual gas in the clearance volume after the exhaust stroke is close to that of air due to lean combustion in diesel engines.

2.3 Engine description and instrumentation

The details of the engine, instrumentation and test conditions that were used are summarized in Tables 1, 2 and 3. Each of the tested fuels (SG0 (baseline diesel), SG10, SG25, and SG45) was tested at the power conditions given in the third column of Table 3. The basic model input data (the P-CAD data) were measured by a pressure sensor and AVL FlexIFEM Indi 601 (2-channel). The pressure data were averaged over 50 cycles and logged by LabView software. The HRR model was solved and analyzed in Microsoft Office Excel software.

Table 1 Engine specifications

Parameter	Specification
Type	4-stroke, single cylinder
Make	Yanmar, 2019 model year, EU Stage V emission compliant,
Rated power	5.7 kW
Speed	3,000 rpm
Bore x Stroke	86 mm x 75 mm
Compression ratio	20.9:1
Displacement	435.66 cm^3
Total cylinder volume	457.55 cm^3
Injection pressure	~20 MPa
Injection timing	13^o bTDC

Table 2 Instrumentation

Parameter	Equipment specification
Cylinder pressure	AVL FlexIFEM Indi 601 (2-channel), AVL GH14D transducer
Fuel consumption (Diesel)	Scale (ADAM CPW plus-35)
Syngas flow	Omega FMA-1622
Temperature	K-type thermocouples

Table 3 Test conditions

Test	Dual fuel	Power, kW	Syngas substitution of diesel, % by energy	Equivalent syngas flow, kg/h	Diesel flow, kg/h
1	SG0	1	0	0	0.745
2		2	0	0	0.925
3		3	0	0	1.12
4		4	0	0	1.451
5	SG10	1	10	0.651	0.673
6		2	10	0.806	0.832
7		3	10	0.976	1.008
8		4	10	1.267	1.307
9	SG25	1	25	1.627	0.558
10		2	25	2.016	0.695
11		3	25	2.437	0.839
12		4	25	3.164	1.091
13	SG45	3	45	4.388	0.616
14		4	45	5.695	0.799

2.4 Fuel properties

The properties of the diesel and syngas fuels are given in Tables 4 and 5 respectively. The selected properties of the ULSD fuel (red diesel) used in the test complied with BS2869 (2010) Class A2. A simulated syngas produced by BOC was used with a heating value of 5.047 MJ/kg.

Table 4 Properties of diesel

Property	**Diesel**
Kinematic viscosity @ 40 ^oC, mm^2/s	~2.7
Density @ 15 ^oC, kg/m^3	840
Cetane Number (CN)	~48
LHV, MJ/kg	~44
Sulphur content, wt%	<10

Table 5 Composition of simulated syngas

Component	**Mol %**	**Molar weight, kg/kgmol**	**LHV, MJ/kg**
Hydrogen	15	2.016	121
CO	20	28.01	10.8
CH_4	4	16.04	50
O2	0.98	32	-
CO_2	12	44.01	-
N_2	48.02	28.01	-

2.5 Determination of the Start of Combustion (SoC) and the End of Combustion (EoC)

The Cumulative Heat Release (CHR) profiles were determined from the modelled HRR profiles for the tested conditions. Thereafter, the fuel burn profiles were determined from the

HRR and the CHR profiles. The Start of Combustion (SoC) was determined for each of the tested modes by direct inspection of the HRR profile, the first and the second derivatives of the measured P-CAD data, p' and p'' respectively. The SoC was taken as the points on the derivatives where the curves were minimum and then followed by a sudden, consistent rise in value. The End of Combustion (EoC), on the other hand, was the crank angle at which the fuel burn profile began to level off after the MFB50.

3. Results and discussion

3.1 Estimated instantaneous volume of the cylinder

Figure 1 presents the estimated instantaneous volume of the cylinder of the engine. The volumes of the cylinder of the engine at the BDC (total volume) and at the TDC (clearance volume) were ~458 cm^3 and ~22 cm^3 respectively.

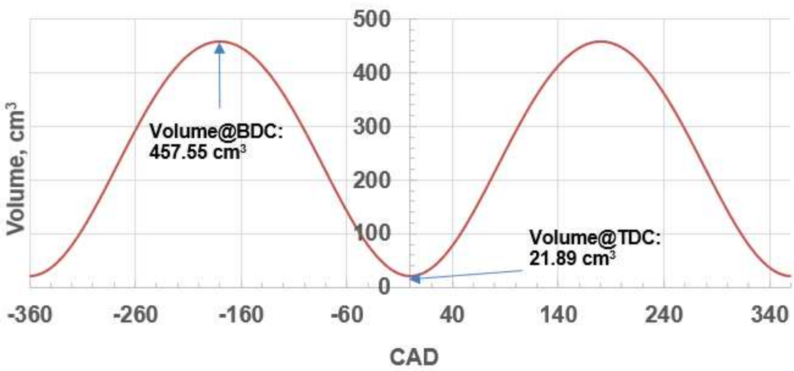

Fig. 1 Instantaneous volume of the cylinder of the Gen-set engine

3.2 Estimated properties of the simulated syngas

The data in Table 5 were used to estimate the stoichiometric AFR ($\mathrm{AFR}_{\mathrm{stoich\_syngas}}$), the density, and the Lower Heating Value (LHV) of the syngas. One (1) mole of syngas was taken as the basis for the estimates. The estimated average molar weight of the simulated syngas was 25.593 kg/kmol while the estimated stoichiometric AFR, density, and LHV were 1.316 by mass, 1.067 kg/m^3, and 5.047 respectively. The details of the estimates are given in the Appendix (Tables A.2 and A.3).

3.3 Pressure-crank angle data

The pressure-crank angle data of the tested conditions were the basic model input data for the diesel-syngas dual-fuel engine HRR analysis that was carried out. Figure 2 presents the basic input data. Figure 2 graphically depicts the potential of diesel-syngas dual fuels to reduce the Peak Pressure (PP) in dual-fuel RCCI engines. As shown in the figure, the PP values for the tested dual fuels (SG10, SG25, and SG45) decreased below the baseline (SG0) as the fraction of syngas increased in the dual fuels. Also, the crank angle timing of the PP increased above the baseline as the flow rate of the syngas increased at constant energy. This was due to the relatively low CN of syngas compared to pure diesel. Generally, the peak pressures increased for each of the tested fuels as the power of the engine was increased. Furthermore, contrary to what was reported by Guo et al. [9], Figure 2 shows that the PP decreased below the baseline as the fraction of syngas increased.

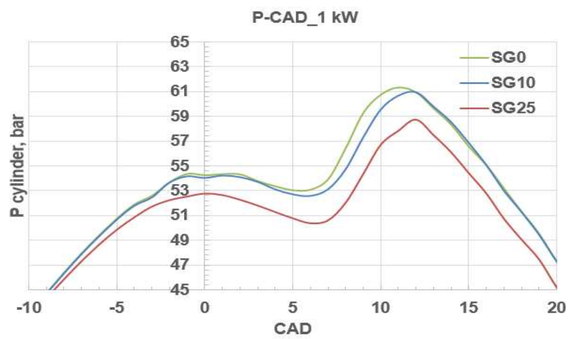

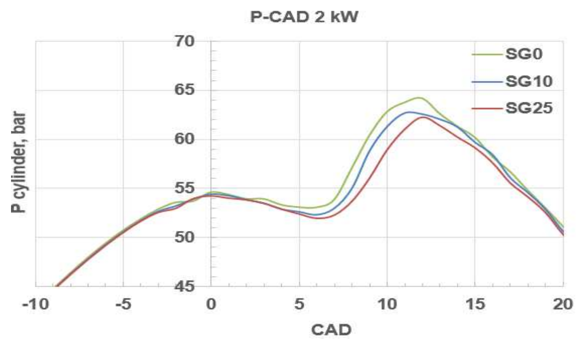

(a) (b)

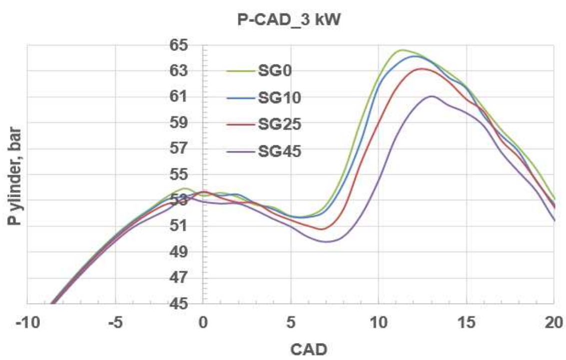

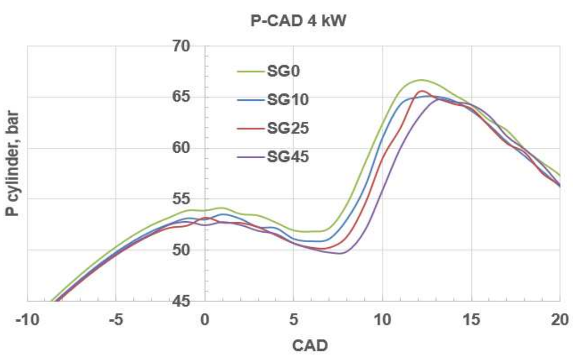

(c) (d)

Fig. 2 Pressure traces for the dual fuels at the tested conditions

3.4 Calculated instantaneous cylinder temperatures

The calculated in-cylinder temperatures are presented in Figure 3. Figure 3 shows that, at each of the tested loads, the temperature of the flame decreased below baseline diesel as the fraction of the syngas in the dual fuel was increased. As was the case for the PP, the Peak Temperature (PT) also increased for each of the tested fuels as the load on the engine was increased.

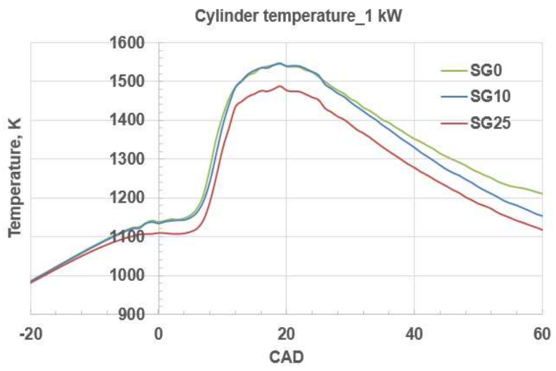

(a)

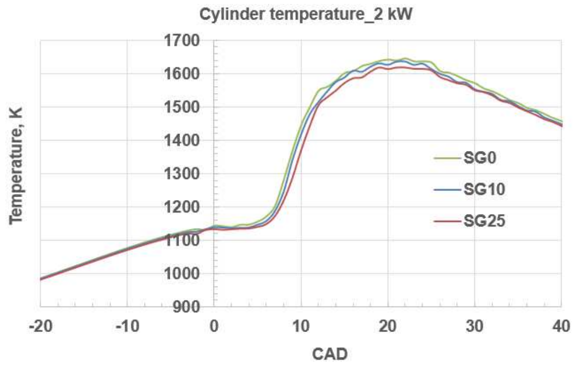

(b)

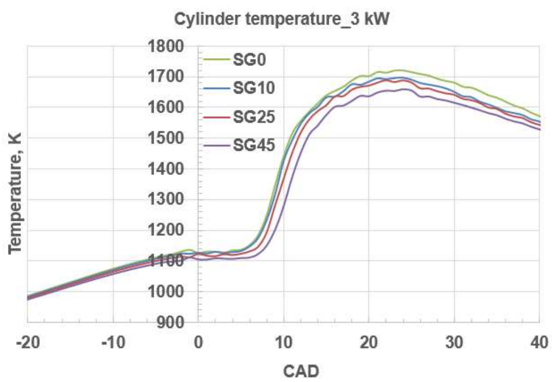

(c)

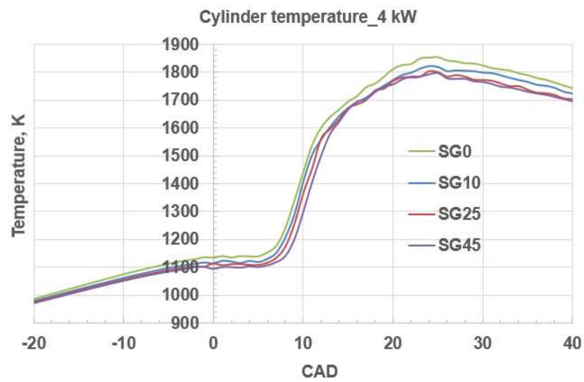

(d)

Fig. 3 Modelled in-cylinder temperatures

3.5 Estimated global excess air ratio, λ_g

The values of the global excess air ratio, λ_g for the diesel-syngas dual-fuel RCCI engine were estimated from Equations 1 and 5 and compared graphically as shown in Figure 4. It shows that, for dual fuel operations at the relatively high loads, the values estimated for the λ_g by Equation 1 deviated drastically from the values estimated by Equation 5 (the improved equation for λ_g). Furthermore, the estimated values of λ_g for the engine from Equation 1 were near-stoichiometric at 4 kW for the tested diesel-syngas dual fuels (SG10, SG25, and SG45). Diesel engines are known to operate in lean combustion mode. Therefore, the improved equation for λ_g which is based on the trapped masses of the gases and diesel fuel (Equation 5) is more accurate than the equation that is based on the flow rates of the fuels and air (Equation 1).

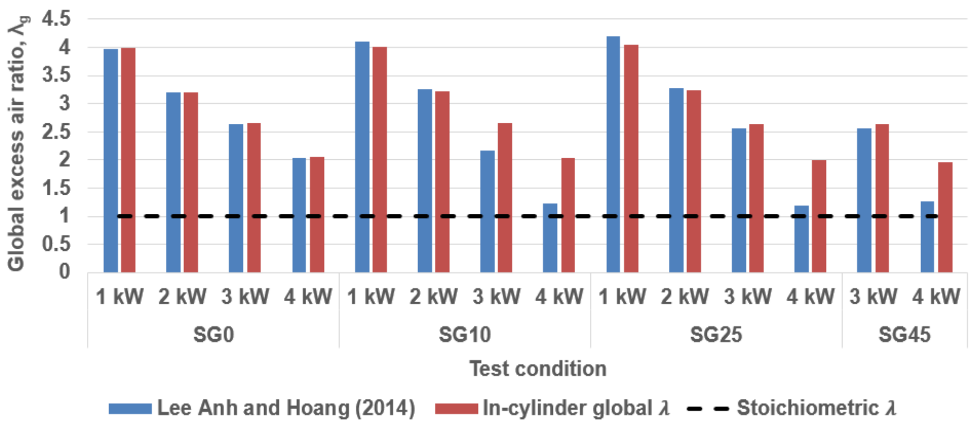

Fig. 4 Comparison of the estimated values of the global excess air ratio, λ_g

Figure 4 shows that as the load on the engine increased for each of the tested fuels, λ_g decreased (the combustion became richer). This was due to the increase in the masses of the diesel-syngas dual fuel as the load on the engine was increased. The increase in the flow rate and the trapped mass of the syngas led to a decrease in the trapped mass of air. Consequently, λ_g decreased as the power of the engine increased.

3.6 Comparison of the modified γ function and the γ functions from literature for diesel-syngas dual fuels

The modified γ function (γ_{mod}) and the γ functions from literature were compared graphically as shown in Figure 5 (for 25% and 45% syngas substitution at 2 kW and 4 kW respectively).

Gamma1 to Gamma4 in Figure 5 represent the γ models of Gatowsky et al. [15], Brunt and Emtage [16], Egnell [17], and Blair [18] respectively while Gamma_mod represents the modified γ function. Figure 5 shows that the values of γ estimated from γ_{mod} for the diesel-syngas dual-fuel RCCI engine were higher than the γ values estimated from the models from literature that expressed $\gamma(\mathrm{T})$. This implies that γ also has a strong dependence on λ for diesel-syngas dual-fuel RCCI engines. The same trend shown in Figure 5 was observed for all the tested modes.

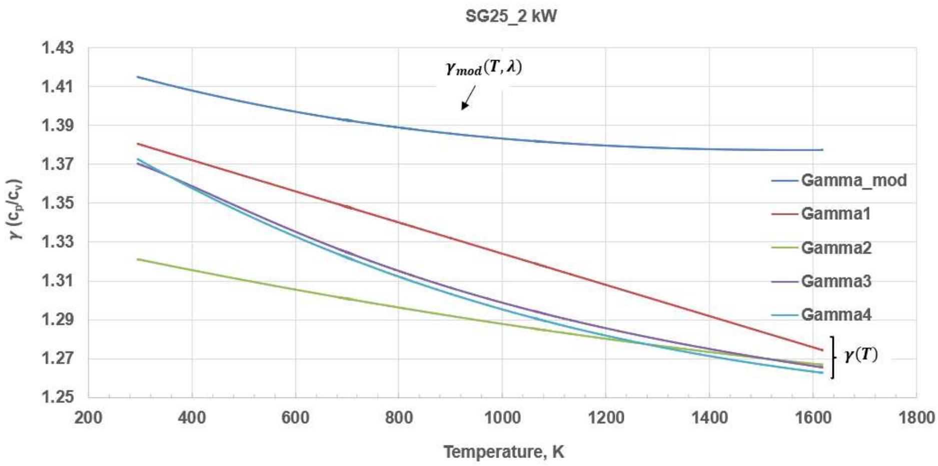

(a)

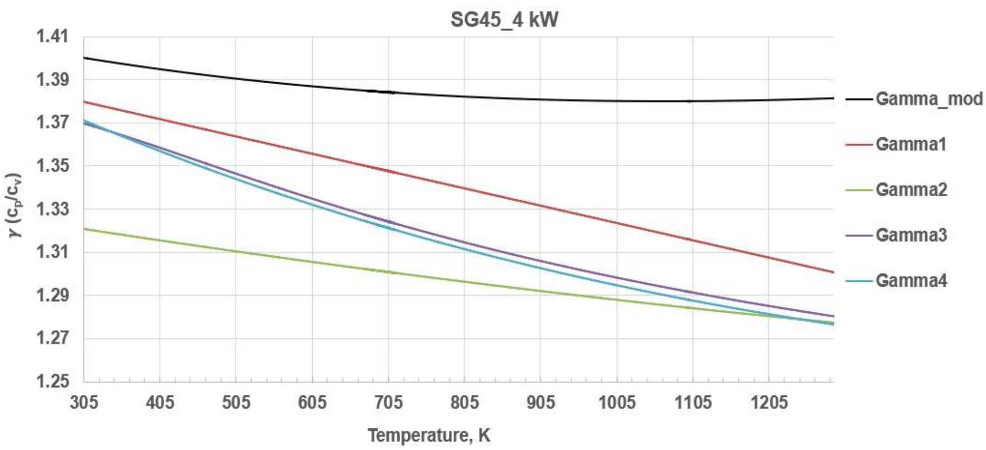

(b)

Fig. 5 Comparison of the modified γ function (γ_{mod}) to the γ functions from literature (a) SG25_2 kW mode (b) SG45_4 kW mode

3.7 Sensitivity of diesel-syngas dual-fuel RCCI engine HRR model to γ functions

The HRR profiles which were derived from the investigated γ and HRR models are shown in Figures 6 to 9. Figures 6 depicts the modelled HRR profiles for pure diesel (SG0) while the HRR profiles for SG10, SG25, and SG45 are depicted in Figures 7, 8, and 9 respectively. HRR1, HRR2, HRR3, and HRR4 were respectively based on the four γ functions from literature (Gamma1 to Gamma4).

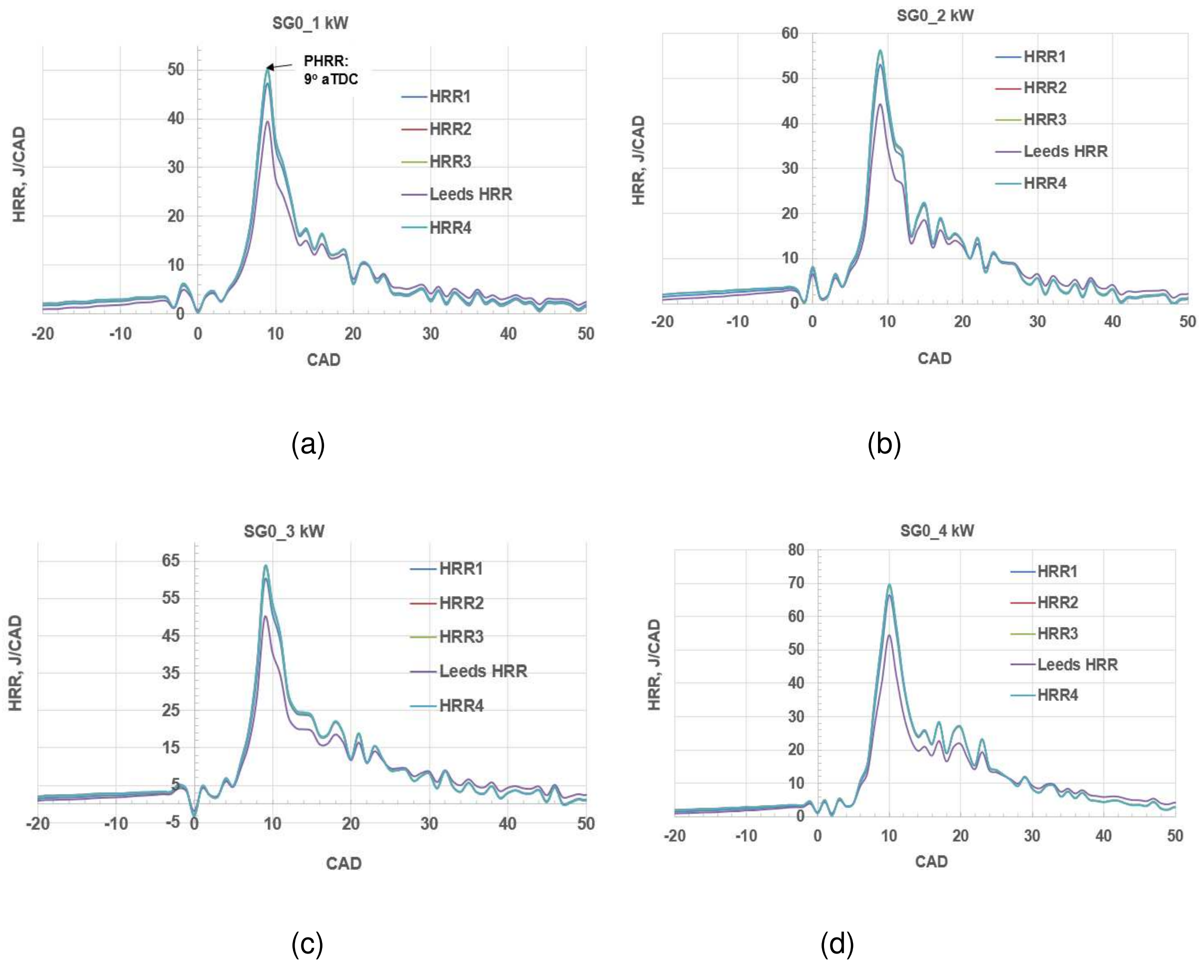

Fig. 6 Modelled HRR profiles for pure diesel (SG0)

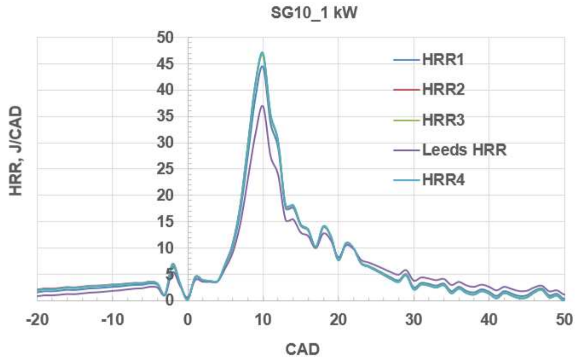

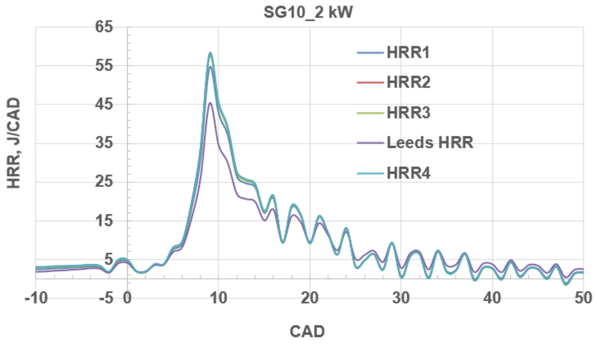

(a) (b)

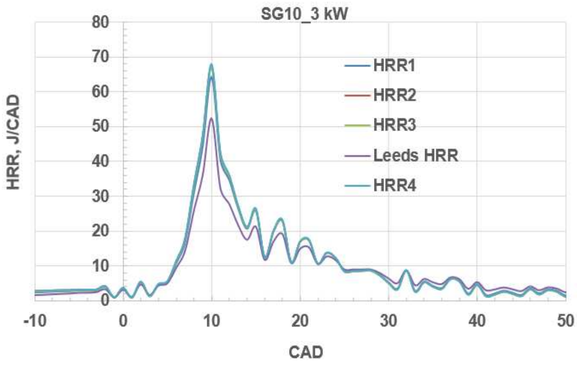

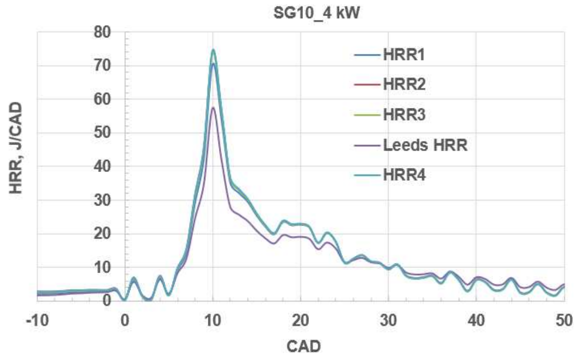

(c) (d)

Fig. 7 Modelled HRR profiles for SG10

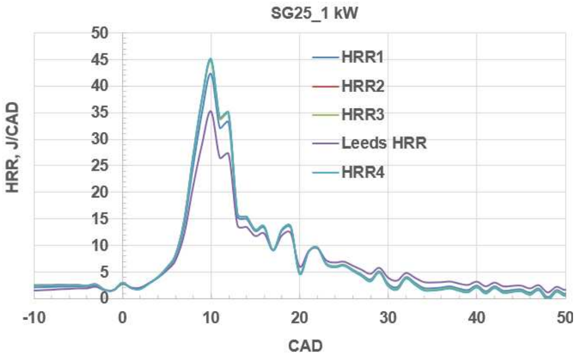

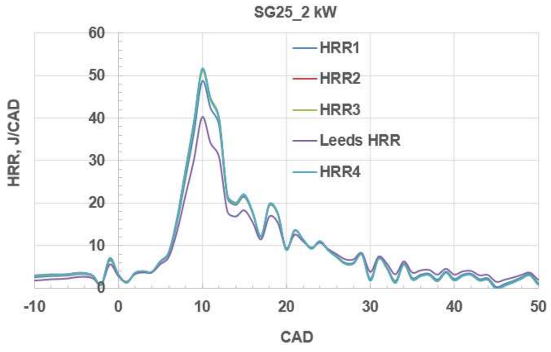

(a) (b)

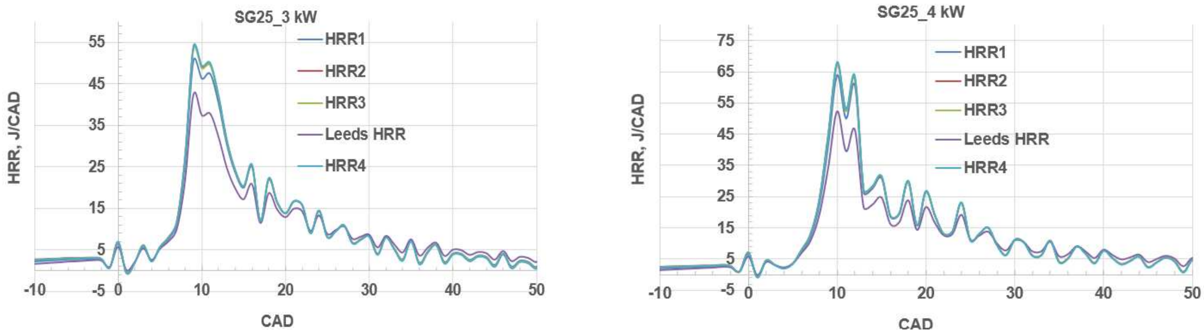

(c) (d)

Fig. 8 Modelled HRR profiles for SG25

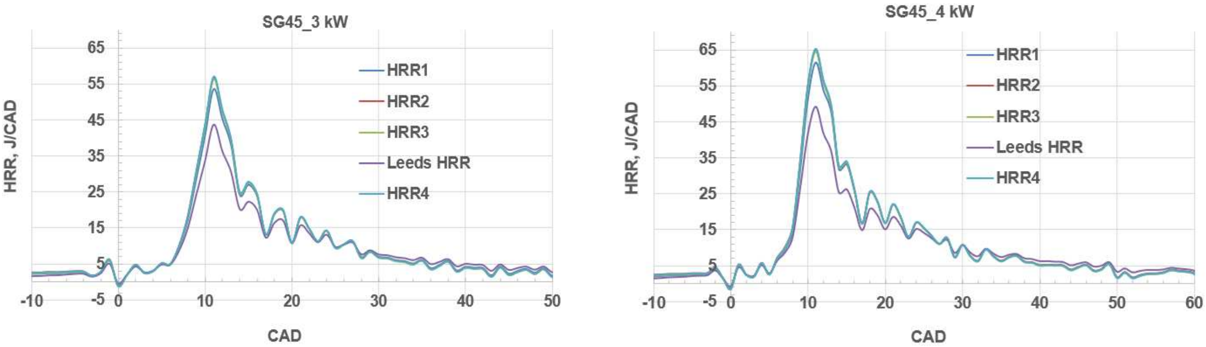

(a) (b)

Fig. 9 Modelled HRR profiles for SG45

The sensitivity of the HRR model of the dual-fuel RCCI engine to γ functions is clearly depicted in the figures as different PHRR values were predicted by the five HRR models for the same engine mode. The Leeds HRR model predicted the lowest PHRR for all the tested dual fuels and power conditions. Figure 5 shows that $\gamma(T,\lambda)$ gives estimates of γ that are higher than the estimates from the functions that expressed $\gamma(T)$. However, Figures 6 to 9 show that, for both baseline diesel and the diesel-syngas dual fuels, the HRR model that utilized $\gamma(T,\lambda)$ predicted lower PHRR values for the dual-fuel RCCI engine than the HRR models that utilized $\gamma(T)$. Though the five HRR models showed the same trend, they predicted different PHRR for the tested dual fuels and engine loads, just as in the cases of single-fuel ULSD and the alternative diesel operations [5,6]. The observed differences in the PHRR predictions of the investigated HRR models necessitated the validation of the Leeds HRR model for the diesel-syngas dual-fuel RCCI engine.

3.7.1 Validation of the Leeds HRR model

The Cumulative Heat Release (CHR) profiles for the tested dual fuels and power conditions were derived from the HRR profiles (strictly for the heat that was released as a result of the combustion of the injected fuel masses). Figure A.1 presents the CHR profiles for the tested dual fuels and power conditions. The HRR and CHR profiles for the tested conditions were used to predict the fuel input energy of the dual-fuel RCCI engine per thermodynamic cycle. The fuel energy input (in J/thermodynamic cycle) predicted by the Leeds HRR model and the HRR models that were based on $\gamma(T)$ were compared to the measured fuel energy input to validate the models. Figure 10 presents the result of the validation of the HRR models. The analysis which was carried out to compare the predicted fuel energy input to the measured fuel energy input is summarized in Table A.4.

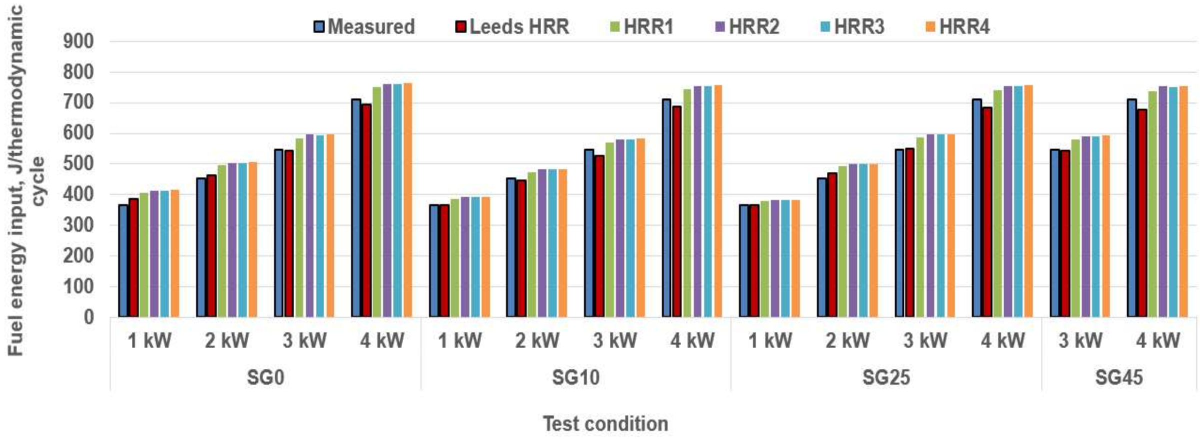

Fig. 10 Comparison of the measured and the predicted fuel energy inputs for the investigated diesel-syngas dual fuels

The red bars with dark borderline in Figure 10 represent the values of the fuel energy input predicted by the Leeds HRR model. The Leeds HRR model predicted the fuel input energy of the dual-fuel RCCI engine for baseline diesel (SG0), SG10, SG25, and SG45 at the tested conditions of power with an overall average (absolute) error of 2.41% compared to the measured fuel energy input (blue bars with black borderline). The percentage errors of the fuel energy input predicted by the Leeds HRR model ranged from -4.59 to +5.41, with a standard deviation of 1.65. The overall average errors which were obtained for off–road diesel and the alternative diesel fuels (GTL and HVO diesels) for a 96 kW Multiple Fuel Injection Strategy (MFIS) IVECO diesel engine were 1.41% and 4.86% respectively [5,6]. The overall average errors in the predicted fuel energy input by the other HRR models that were based on γ(T) ranged from 6.26 to 8.29%. The HRR models that were based on γ(T) overpredicted the fuel consumption of the diesel-syngas dual-fuel engine because the significant effect of λ on γ was not considered in the models. Figure 10 clearly shows that the accuracy of the HRR model of diesel engines for predicting the combustion behaviour of diesel-syngas dual fuels in the dual-fuel RCCI diesel engine was enhanced by using γ(T, λ).

3.7.2 Effect of syngas substitution of diesel at constant energy on the combustion behaviour of RCCI diesel engines

The effect of syngas substitution of diesel on the combustion behaviour of diesel engines was investigated by plotting the HRR profiles for the tested dual fuels on the same graph for each of the tested engine loads. The three phases of the combustion of the injected diesel-syngas fuel masses in the cylinder of the dual-fuel engine [7] are depicted in Figure 11 for 25% syngas substitution of diesel at 1 kW. The rate of release of heat during the rapid/premixed combustion phase (phase A) was the highest. The heat that was released in stage A was due to the premixed combustion of the DI diesel and some of the injected syngas. The first HRR peak (P1) in Figure 11 resulted from the premixed combustion of the pilot injection fuel (diesel). Stage B resulted from the premixed combustion of the port injected fuel (syngas) as well as the remaining diesel. The second HRR peak (P2) in Figure 11 resulted from the premixed combustion of syngas. The HRR reduced drastically during the mixing-controlled combustion phase (phase C) as the combustion became less spontaneous than it was in the previous stages.

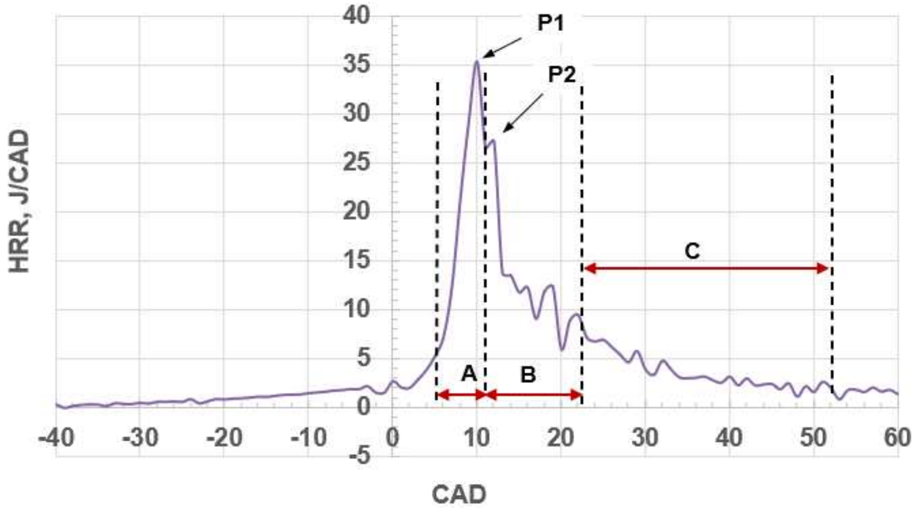

Fig. 11 Stages of the combustion of the diesel-syngas dual-fuel in the RCCI engine

Figure 12 depicts the effect of increasing the fraction of syngas in the dual fuel and the load on the engine on the combustion behaviour of the RCCI engine. Generally, it was observed in Figure 12 that, as the fraction of syngas increased for each of the tested conditions of power, the HRR profiles of the dual fuels (SG10, SG25, and SG45) shifted to the right of the profile for baseline diesel (SG0). This was because the tendency of the dual fuel to auto-ignite (the effective CN of the dual fuel) decreased as the fraction of syngas was increased. The relatively low CN of syngas increased the ID of the dual fuels as the syngas fraction increased. As a result of the observed increase in the ID for the diesel-syngas dual fuels above the baseline, the PHRR (and the PP; Figure 2) for the dual fuels (SG10, SG25, and SG45) occurred later than pure diesel (SG0). Rith et al. [12] also reported that the PHRR occurred later than baseline diesel as the flow rate of syngas was increased.

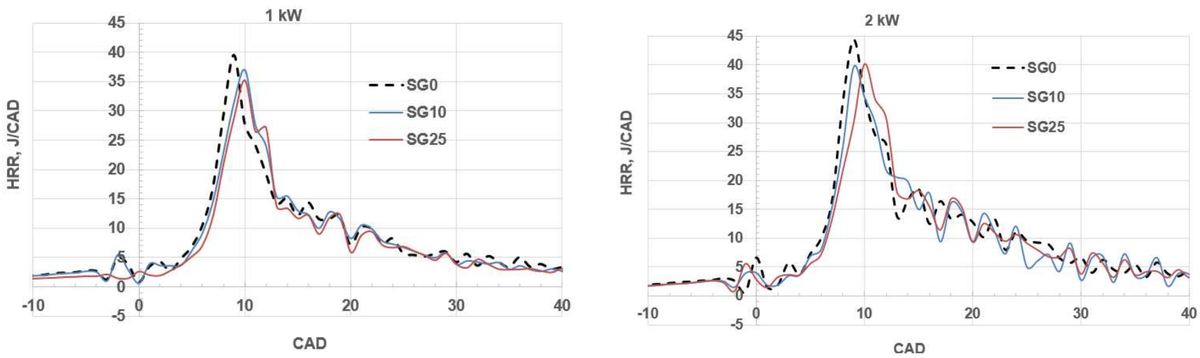

(a) (b)

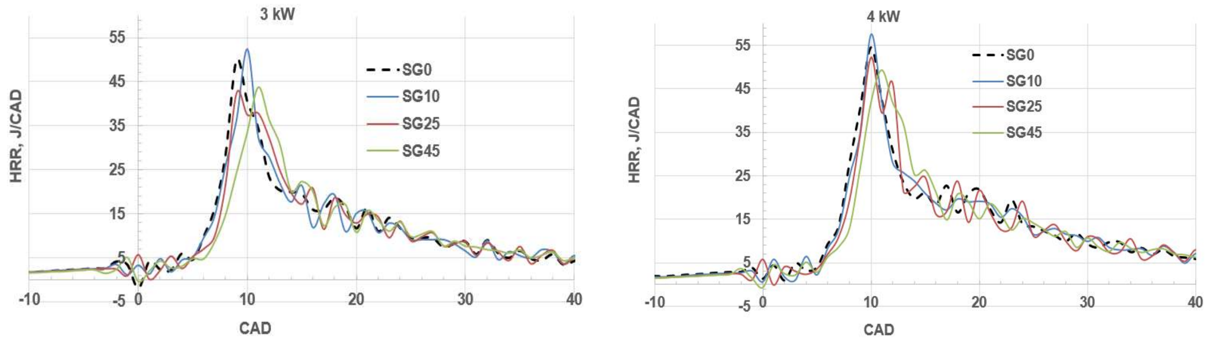

(c) (d)

Fig. 12 Effect of syngas concentration on the combustion behaviour of the diesel-syngas dual-fuel RCCI engine

Furthermore, Rith et al. [12] reported that the PHRR decreased below the baseline as the fraction of syngas increased. Contrary to what was reported by the authors, Figure 12 shows that at the relatively high load conditions (3 and 4 kW), the values of the PHRR for the lowest syngas fraction (SG10) were higher than those for pure diesel (SG0). The observed high PHRR for SG10 above the baseline could be because the premixed combustion of diesel (represented by P1 in Figure 11) and the premixed combustion of the port injected syngas (P2 in Figure 11) occurred at the same crank angle at the lowest syngas fraction (SG10).

3.7.3 Combustion phasing for the diesel-syngas dual fuel RCCI engine

The Start of Combustion (SoC), the End of Combustion (EoC), and the MFB50 were determined from the HRR profiles, the derivatives of the P-CAD data, and the derived fuel burn profiles for the tested conditions as shown in Figures 13 and 14. The crank angle timings for the PP, PT and PHRR were determined from the pressure, temperature, and HRR profiles, respectively. Table 6 presents the combustion phasing for the tested conditions. The Duration of Combustion (DoC) was estimated as the difference between the EoC and the SoC.

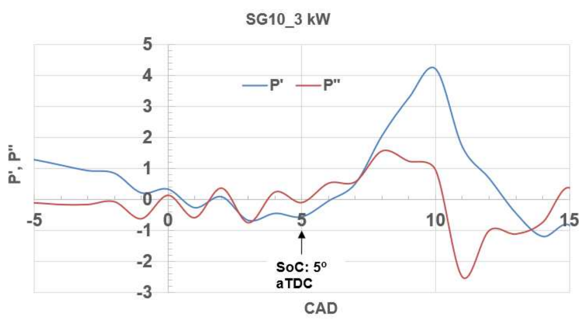

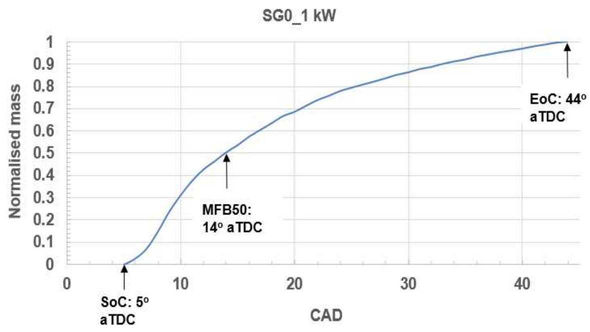

Fig. 13 Determination of SoC: SG10_3 kW Fig. 14 SoC, MFB50, EoC for SG0 at 1 kW

Table 6 Combustion phasing for the tested conditions

		CAD						
Dual fuel	**Power, kW**	**SoC**	**MFB50**	**EoC**	**DoC**	**PP**	**PT**	**PHRR**
SG0	1	5	14	44	39	11	19	9
	2	5	14.5	48	43	12	22	9
	3	5	16	52	47	11	24	9
	4	4	18	67	63	12	26	10
SG10	1	6	14	43	37	12	19	10
	2	6	15	48	42	11	22	9
	3	5	16	50	45	12	24	10
	4	5	19	67	62	13	24	10
SG25	1	6	14.5	53	47	12	19	10
	2	6	16	58	52	12	22	10
	3	5	17	60	55	13	24	9
	4	5	19	67	62	12	24	10
SG45	3	6	17.5	60	54	13	24	11
	4	6	19	65	59	13	25	11

Table 6 shows that the SoC, MFB50, PP, and PHRR occurred later for the diesel-syngas dual fuels compared to pure diesel. Table 6 also shows that the DoC increased above the baseline for the relatively high syngas flow rates (SG25 and SG45). This could be attributed to the delayed and slow combustion of the CO in the syngas.

The values of the Peak Pressure (PP), the Peak Temperature (PT), and the PHRR for the tested conditions are presented in Table A.5. The table shows that the values for the PP, and the PT decreased below the baseline for the tested diesel-syngas dual fuels. This was due to the relatively low Cv of syngas.

3.7.4 Effect of syngas substitution of diesel on the Ignition Delay (ID) of the dual-fuel RCCI engine

The values of the Ignition Delay (ID) for the tested conditions were estimated by adding the corresponding SoC crank angles to the Start of Injection (SoI) crank angle of the engine (13° bTDC). Table 7 presents the estimated values of the ID.

Table 7 Ignition Delay (ID) values for the investigated fuel blends and engine loads

Fuel blend	**Power, kW**	**ID, CAD**	**ID, milliseconds**
SG0	1	18	1
	2	18	1
	3	18	1
	4	17	0.94
SG10	1	19	1.06
	2	19	1.06
	3	18	1
	4	18	1
SG25	1	19	1.06
	2	19	1.06
	3	18	1
	4	18	1

SG45	3	19	1.06
	4	19	1.06

The values of the ID for the tested conditions (Table 7) showed that diesel-syngas dual fuels increase the ID in dual-fuel RCCI engines. The results for the ID in the current work contradict what was reported by Garnier et al. [7].

3.8 Estimation of possible CO_2 savings from the utilization of diesel-syngas dual fuel in diesel engines

Table 8 shows that the use of 45% (by energy) syngas substitution of diesel in a typical developing country (Nigeria) can reduce CO_2 emissions by ~0.26 million tonnes per year. The estimate in Table 8 is based on the consumption of diesel in Nigeria for the year 2019 [19] and the maximum syngas substitution that was used in the current work.

Table 8 Possible reduction in CO_2 emissions from the substitution of diesel with syngas

S/n	**Item**	**Calculation**	**Value**
1	Syngas substitution of diesel by energy, %		45
2	Consumption of diesel in Nigeria in 2019 [19], million tonnes	-	0.19
3	CO_2 emission per kg of diesel combusted [20], kg CO_2/kg diesel	-	3.1
4	CO_2 emissions from the combustion of diesel in Nigeria, million tonnes	0.19 x 3.1	0.58
5	Reduction in CO_2 emissions for 45% substitution of diesel by energy, million tonnes	45 x 0.58/100	~0.26

4. Conclusion

In this work, the improved Leeds HRR model was validated and applied to a diesel-syngas dual-fuel RCCI Gen-set engine to investigate the effect of syngas substitution of diesel on the engine. The current work showed that the accuracy of the HRR model of the diesel-syngas dual-fuel RCCI engine was also strongly depended on the specific heats ratio (γ). The effect of the excess air ratio (λ) on γ was also investigated in this work for dual-fuel RCCI diesel engines. λ was found to have a significant effect on γ. In the current work, the accuracy of the Leeds HRR model for the analysis of the combustion behaviour of the dual-fuel RCCI engine was further enhanced by the use of in-cylinder global lambda function (λ_g). The Leeds HRR model based on $\gamma_{mod}(T,\lambda)$ predicted the fuel input energy of the engine with an average (absolute) error of 2.41%. The errors in the fuel input energy predicted by the Leeds HRR model ranged from -4.59 to +5.41%, with a standard deviation of 1.65. The average error in the fuel input energy predictions of the other models which were based on $\gamma(T)$ ranged from 6.26 to 8.29%. The error in the predictions of the other models was because λ was neglected in the models. Therefore, in this work, it was shown that the accuracy of the HRR model of diesel-syngas dual-fuel RCCI engines is enhanced by using $\gamma(T,\lambda)$. It was found that the SoC, MFB50, PP, and PHRR occurred later for the diesel-syngas dual fuels compared to baseline diesel due to the observed increase in the Ignition Delay as the fraction of syngas was increased. It was observed in the current work that diesel-syngas dual fuels led to a decrease in the Peak Pressure (PP) and the Peak Temperature (PT) below the baseline. The current work also showed that 45% by energy substitution of diesel with syngas in Nigeria (a developing country) can potentially reduce CO_2 emissions by ~0.26 million tonnes.

Acknowledgements

This work was supported by the Engineering and Physical Sciences Research Council (EPSRC) for a GCRF grant: Creating resilient sustainable micro-grids through hybrid renewable energy systems (CRESUM-HYRES), grant number EP/R030243/1 and by the

Petroleum Technology Development Fund (PTDF), Nigeria; and the National Agency for Science and Engineering Infrastructure (NASENI), Nigeria.

Appendix

Table A.1 Values of the coefficients in Equation 2 [13]

Coefficients (γ_b)	Values
b_1	1.498119965
b_2	-0.00011303
b_3	-0.26688898
b_4	4.03642e-08
b_5	0.273428364
b_6	5.7462e-05
b_7	-7.2026e-12
b_8	-0.08218813
b_9	-1.3029e-05
b_{10}	2.35732e-08

Table A.2 Stoichiometric AFR of the simulated syngas

Species	**Composition in syngas, mol %**	**Molar mass, kg/kgmol**	**Mass, kg**	**Stoichiometric O_2 requirement, kmol**	**N_2, kmol**	**Air mass, kg**
H_2	0.15	2.016	0.302	0.075	0.282	10.3
CO	0.2	28.01	5.602	0.100	0.376	13.733
CH_4	0.04	16.04	0.642	0.080	0.301	10.987
O_2	0.0098	32	0.314	-0.0098	-0.037	-1,346
CO_2	0.12	44.01	5.281	-	-	-
N_2	0.4802	28.014	13.452	-	-	-
Total	1		25.593			33.674

$\mathrm{AFR}_{\mathrm{stoich\_syngas}}$: 33.674/25.593 = 1.316 kg/kg

Table A.3 Density and the Lower Heating Value (LHV) of the simulated syngas

Species	Composition, mol %	Molar mass, kg/kgmol	Mass, kg	Mass fraction	Density, kg/m^3	LHV, MJ/kg
H_2	0.15	2.016	0.302	0.012	0.0899	121
CO	0.2	28.01	5.602	0.219	1.165	10.8
CH_4	0.04	16.04	0.642	0.025	0.668	50
O_2	0.0098	32	0.314	0.012	1.331	0
CO_2	0.12	44.01	5.281	0.206	1.842	0
N_2	0.4802	28.014	13.452	0.526	1.165	0
Total	1		25.593	1		
Simulated syngas					1.067	5.047

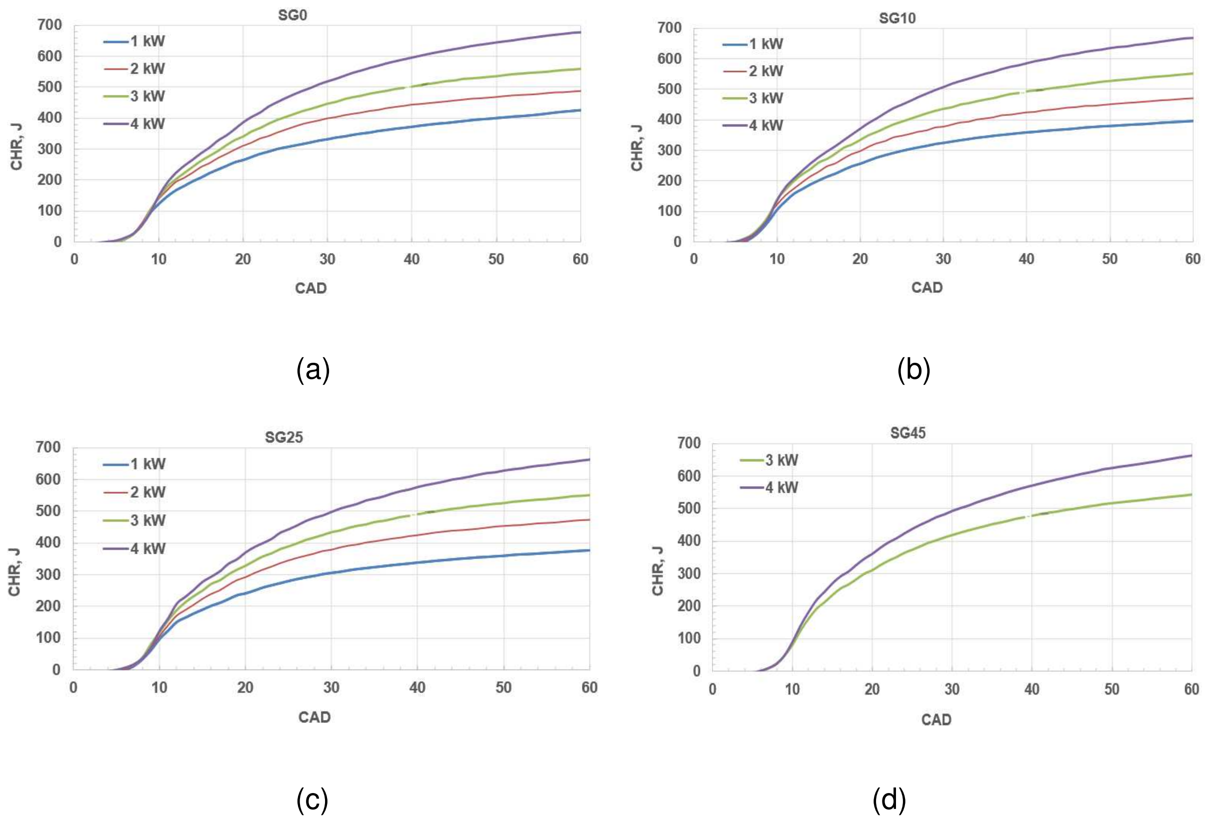

(a) (b)

(c) (d)

Fig. A.1 CHR profiles for the tested fuels

Table A.4 Validation of the Leeds HRR model for diesel-syngas dual fuel RCCI engine

			Energy input, J/thermodynamic cycle						% Deviation from measured input energy				
Dual fuel	Power, kW	Global lambda, λ_g	Measured	Leeds HRR	HRR1	HRR2	HRR3	HRR4	Leeds HRR	HRR1	HRR2	HRR3	HRR4
SG0	1	3.99	364.71	384.45	406.5	414	412.9	414.5	5.41	11.46	13.51	13.21	13.65
	2	3.21	463.5	495.5	488.64	504.4	503.66	505.55	2.49	9.57	11.54	11.37	11.79
	3	2.66	542.42	584.16	595.57	594.6	597	587.25	-0.85	6.78	8.87	8.69	9.13
	4	2.05	709.87	694.76	751.2	762.46	762	764.7	-2.13	5.82	7.41	7.34	7.72
SG10	1	4.01	364.71	365.85	386.9	393.5	392.8	394.1	0.31	6.08	7.89	7.7	8.06
	2	3.22	452.22	445.54	474.17	482.63	481.83	483.56	-1.48	4.85	6.72	6.55	6.93
	3	2.65	547.07	526.37	568.58	580.37	579.32	581.8	-3.78	3.93	6.09	5.9	6.35
	4	2.03	709.87	685.9	742.54	754.84	754	756.9	-3.38	4.60	6.33	6.22	6.63
SG25	1	4.04	364.71	365.68	378	382	381.6	382.46	0.27	3.64	4.74	4.63	4.87
	2	3.23	452.22	469.6	493.03	499.53	498.96	500	3.84	9.02	10.46	10.34	10.57
	3	2.64	547.07	551.3	587.2	597.17	596.3	598.3	0.77	7.34	9.16	9	9.36
	4	2.00	709.87	683.8	741.13	754.1	753.25	756.13	-3.67	4.4	6.23	6.11	6.52
SG45	3	2.63	547.07	543.18	579.94	590.86	589.66	591.87	-0.71	6	8	7.79	8.19
	4	1.96	709.87	677.3	738.7	754.78	751.54	754.6	-4.59	4.06	6.33	5.87	6.3
					Average of absolute error, %:				2.41	6.26	8.09	7.91	8.29

Standard deviation:	1.65	2.28	2.33	2.32	2.32
% error range:	-4.59 - +5.41	3.64 – 11.46	4.74 – 13.51	4.63 – 13.21	4.87 – 13.65

Table A.5 Model results for the Peak Pressure (PP), Peak Temperature (PT), and Peak Heat Release Rate (PHRR) for the tested dual fuels

Dual fuel	Power, kW	PP, bar	PT, K	PHRR, J/CAD
SG0	1	61.31	1548.07	39.5
	2	64.14	1646.54	44.3
	3	64.45	1719.39	49.95
	4	66.66	1840.84	54.42
SG10	1	60.96	1544.57	36.95
	2	62.66	1636.71	45.36
	3	64.17	1696	52.37
	4	65.01	1822.95	57.5
SG25	1	58.7	1488.23	35.27
	2	62.24	1617.32	40.15
	3	63.03	1687.08	42.4
	4	65.48	1802.12	52.2
SG45	3	61.07	1658.01	43.7
	4	64.71	1796.52	49.25

References

[1] Aslam Z, Li H, Hammerton J, Andrews GE, Ross A, Lovett JC. Increasing access to electricity: An assessment of the energy and power generation potential from biomass waste residues in Tanzania. Energies 2021; 14: 1793. https://doi.org/10.3390/ en14061793.

[2] San-Akca B, Sever SD, Yimaz S. Does natural gas fuel civil war? Rethinking energy security, international relations, and fossil-fuel conflict. Energy Research and Social Science 2020; 70: 101690. https://doi.org/10.1016/j.erss.2020.101690.

[3] Acharya B, Adhikari S. Household energy consumption and adaptation behavior during crisis: Evidence from Indian economic blockade on Nepal. Energy Policy 2021; 148: 111998. https://doi.org/10.1016/j.enpol.2020.111998.

[4] Heywood JB. Internal combustion engine fundamentals. New York: McGraw-Hill; 1988.

[5] Olanrewaju FO, Li H, Andrews GE, Herodotos NP. Improved model for the analysis of the heat release rate (HRR) in compression ignition (CI) engines. J Energy Institute 2020; 93:1901-13. https//doi.org/10.1016/j.joei.2020.04.005.

[6] Olanrewaju FO, Wu Y, Li H, Andrews GE, Herodotos NP. An improved heat release rate (HRR) model for the analysis of combustion behaviour of diesel, GTL, and HVO diesel. SAE technical paper 2020-01-2060; 2020. https//doi.org/10.4271/2020- 01-2060.
[7] Garnier C, Bilcan A, Le Corre O, Rahmouni, C. Characterisation of a syngas-diesel fuelled CI engine. SAE technical paper 2005-01-1731; 2005. https//doi.org/10.4271/2005-01-1731.
[8] Le Anh T, Hoang L. Simulation of a syngas-diesel dual fuel engine for small-scale power generator. J Sci & Tech 2014; 100B:36-41.
[9] Guo H, Neill WS, Liko B. The combustion and emissions performance of a syngas-diesel dual fuel compression ignition engine. ASME paper no. ICEF2016-9367; 2016. https://doi.org/10.1115/ICEF2016-9367.
[10] Mahgoub BKM, Hassan S, Sulaiman SA, Mamat R, Abdullah AA, Hagos FY. Combustion and performance of syngas dual fueling in a CI engine with blended biodiesel as pilot fuel. J BioResources 2017; 12(3):5617-31.
[11] Kousheshi N, Yari M, Paykani A, Saberi Mehr A, de la Fuente G. Effect of syngas composition on the combustion and emissions characteristics of a syngas/diesel RCCI engine. J Energies 2020; 13: 212. https//doi.org/10.3390/en13010212.
[12] Rith M, Buenconsejo B, Gitano-Briggs H, Biona JBM. Design and fabrication of a low-cost research facility for the study of combustion characteristics of a dual producer gas-diesel engine. J Engineering and Applied Science Research 2020; 47:447-57. https//doi.org/10.14456/easr.2020.48.
[13] Ceviz MA, Kaymaz I. Temperature and air–fuel ratio dependent specific heat ratio functions for lean burned and unburned mixture. J Energy Conversion and Management 2005; 46(15):2387-404. https://doi.org/10.1016/j.enconman.2004.12.009.
[14] Rajkumar M. Heat release analysis and modeling for a common-rail diesel engine. MSc thesis, Mechanical Engineering, University of Tennessee – Knoxville, https://trace.tennessee.edu/cgi/viewcontent.cgi?article=3523&context=utk_gradthes2002 [accessed 28 April 2021].
[15] Gatowski JA, Balles EN, Chun KM, Nelson FE, Eckchian JA, Heywood, JB. Heat release analysis of engine pressure data. SAE paper no. 841359; 1984. https://doi.org/10.4271/841359.
[16] Brunt MFJ, Emtage AL. Evaluation of Burn Rate Routines and Analysis Errors. 1997, SAE paper no. 970037; 1997. https://doi.org/10.4271/970037.
[17] Egnell R. Combustion diagnostics by means of multizone heat release analysis and no calculation. SAE paper no. 981424; 1998. https://doi.org/10.4271/981424.
[18] Blair GP. The basic design of two-stroke engines. Warrendale PA (United States): Society of Automotive Engineers; 1990.
[19] NNPC. Annual statistical bulletin. https://nnpcgroup.com/NNPCDocuments/Annual%20Statistics%20Bulletin%E2%80%8B/2019%20ASB.pdf 2019. [accessed 9 August 2021].
[20] FR. Carbon emissions of different fuels. https://www.forestresearch.gov.uk/tools-and-resources/fthr/biomass-energy-resources/reference-biomass/facts-figures/carbon-emissions-of-different-fuels/. 2021 [accessed 7 August 2021].